Bulletin of the Seismological Society of America, Vol. 87, No. 3, pp. 589–605, June 1997

Regional Seismic Discriminants Using Wave-Train Energy Ratios

by Bradley B. Woods and Donald V. Helmberger

Abstract We have examined broadband regional waveforms of recent (since 1988) Nevada Test Site (NTS) underground explosions and earthquakes throughout the southwestern United States and Baja, Mexico, recorded by TERRAscope and other IRIS stations in order to characterize seismic sources for the purposes of event identification. As expected, earthquakes tended to be richer in long-period surface-wave and short-period shear-wave energy relative to explosions of comparable *P*-wave strength. Also, explosions, in general, were found to be richer in 1- to 6-sec surface-wave (*Rg*) energy and other late-arriving coda energy than were earthquakes. Most earthquakes show relatively little long-period ($T > 6$ sec) *Rg* and surface-wave coda energy, which we attribute to their deeper source depths, whereas known shallow earthquakes do exhibit these phases. We have developed several seismic discriminants based on our observations. The most promising discriminant is the ratio of short-period ($f \geqq 1.0$ Hz), vertical component, P_{nl} wave-train energy (E_{spPz}) to long-period (0.05 to 0.167 Hz), three-component, surface-wave energy (E_{lp-3}). For this ratio, explosions tend to have a higher value than do earthquakes. This discriminant works on the same premise as the teleseismic m_b:M_S ratio, for which earthquakes are richer in long-period surface-wave energy relative to explosions with the same body-wave magnitude. The long-period passband was chosen to limit the effect of longer-period noise and to remove the effect of the coda surface waves. Another potential discriminant examined is the ratio of short-period ($f \geqq 1.0$ Hz), vertical-component, *P*-wave to *S*-wave energy (E_{spPz}:E_{spSz}). We find that this criterion only yields marginal separation of the source populations but becomes more effective at higher frequency bands ($f \geqq 4.0$ Hz) or when looking at single-station observations. It does, however, help to quantify significant short-period waveform differences between the three test subsites, with Pahute Mesa shots generating relatively little *S*-wave energy compared to those of Yucca Flat for which the *S* wave (or *Lg*) is often the largest phase, while Rainier's shots are intermediate in character with distinct but less prominent *S* waves. This *S*-wave generation is thought to be caused by near-source scattering to converted phases and appears to be highly dependent on the near-source geology. These two discriminants are useful in that they are simple and fast to calculate. Using regional stations for sources 200 to 1300 km away, the magnitude threshold for the E_{spPz}:E_{lp-3} discriminant is roughly $M_L \geqq 4.0$, the limiting factor being the signal level of the Airy phase, while that for the E_{spPz}:E_{spSz} discriminant is roughly $M_L \geqq 3.0$ for the same distance ranges.

Introduction

Recent studies of regional seismic data (Woods *et al.*, 1993; Patton and Walter, 1993; Taylor *et al.*, 1989) support teleseismic observations that explosive sources tend to be significantly richer in short-period (~1 Hz) *P*-wave energy than earthquakes, relative to their long-period (0.05 to 0.167 Hz) surface-wave energy, as manifested in the m_b:M_S discriminant (Basham, 1969; Lieberman and Pomeroy, 1969; Marshall *et al.*, 1971; Stevens and Day, 1985). Extending such short-period:long-period (SP:LP) measures to regional distances lowers the effective discrimination magnitude threshold, thus making this type of discriminant more useful.

From visual inspection of broadband displacement recordings of regional earthquakes and explosions, it is apparent that these two source types show distinctly different spectral content as is shown in Figure 1, which compares records from the Joint Verification Experiment Kearsarge and the Lee Vining and Little Skull Mountain earthquakes. The three events, all recorded at Pasadena, California (PAS),

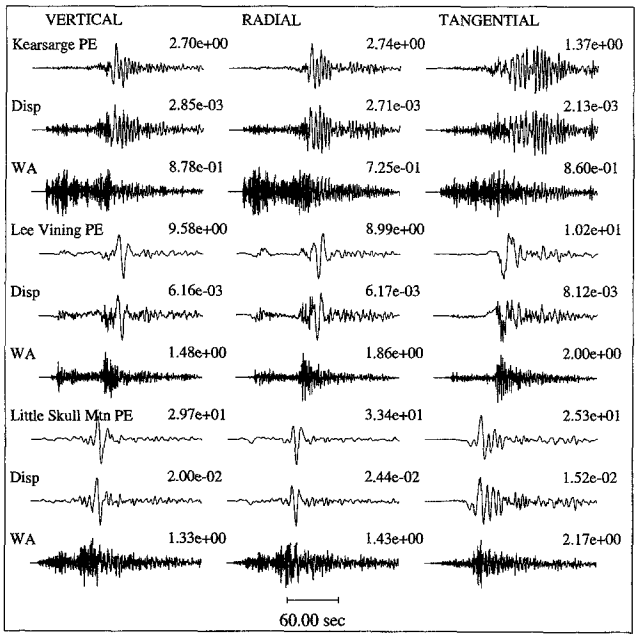

Figure 1. Regional waveform comparisons of the U.S. JVE Kearsarge with comparable-sized earthquakes (Lee Vining and Little Skull Mountain) at similar distances (after Woods *et al.*, 1993). Each set of three rows of three-component records is for one event; the first row traces are convolved with a long-period Press-Ewing (PE) instrument, the second row are broadband (BB) displacements, and the third row of traces are convolved with a short-period Wood-Anderson (WA) instrument. The peak amplitude (cm) of each trace is given to its right.

are at roughly equal epicentral distances (Kearsarge, 388 km; Little Skull Mtn, 321 km; and Lee Vining, 442 km). Their locations are shown in the shaded inset in Figure 2. Source information is given for them in Table 1. The three-component averaged-ratio of peak short-period (WA) to long-period (PE) amplitude is 0.405 for the explosion. For the earthquakes, it is lower, being 0.195 for Lee Vining and 0.0585 for Little Skull Mountain. This measurement reflects the relative strength of body-wave to surface-wave generation. Should the peak short-period amplitude be measured solely in the P wave-train window, this ratio would be lower still for earthquakes, thus separating them further from explosions. This feature is consistent with other observations that earthquakes tend to be long-period rich relative to explosions with similar short-period energy levels.

There are a number of factors that contribute to this difference in waveform characteristics between earthquakes and explosions. This contrast can be explained, in part, by the differences in characteristic source-time functions and spatial source dimensions between earthquakes and explosions. Savino *et al.* (1971), Aki *et al.* (1974), and Müller (1973) find that explosions exhibit characteristics, in part, of an impulsive source and are, in any case, impulsive and compact sources relative to earthquakes (Walter *et al.*, 1995). Empirical explosion source models developed by Haskell (1967) and Mueller and Murphy (1971) yield source time functions with rise times that are only fractions of second in length. These source time functions are steplike in nature, with overshoot giving the explosion source an impulselike character. Aki (1967), Brune (1970), and Marshall (1970) find that earthquake source functions, on the other hand, are best-modeled as ramps or step functions with combined duration and rise times greater than 1 sec. Dreger and Helmberger (1991) found that even moderate-sized earthquakes ($M_L \sim 5.2$) have source durations greater than 1 sec. Thus differences in the source processes and dimensions between earthquakes and explosions help to explain the differences in their observed spectra.

Stevens and Day (1985) conclude from numerical modeling experiments that the difference between earthquake and explosion source spectra is only partially responsible for explaining m_b:M_S observations, as at lower magnitudes ($m_b \leqq 4.5$), the source spectral characteristics converge. They also cite focal mechanism, near-source elastic properties, and pP interference effects as contributing factors to the separation of populations with this type of discriminant. The effect of earthquake focal mechanism upon the relative excitation of P waves and surface waves can, of course, be significant, but it is also highly variable; in their study, they found that the effect of earthquake focal mechanism on P-wave and Rayleigh-wave amplitude does, on average, help to separate them from explosions but that the scatter due to fault orientation is even larger. In a theoretical study of regional m_b:M_S, Lilwall (1988) found that earthquakes with a large dip-slip component do show some separation from explosions but that strike-slip events, on average, do not.

The two above-mentioned studies found that the primary explanation for the difference in relative excitement of P waves and Rayleigh waves between earthquakes and explosions is due to the low-velocity source medium for explosions. Stevens and Day show that the difference between $m_b - M_S$ of an explosion and earthquake involves the factors $(\rho_q\alpha_q^3/\rho_x\alpha_x^3)^{1/2}$ and α_x^2/β_x^2, where the subscript q denotes earthquake and x denotes explosion. The effect of the first term can be considered a depth-related phenomenon, whereby shallow sources in low-velocity material (usually explosions) generate relatively larger body-wave to surface-wave amplitude ratios than do deeper events. By their nature, earthquakes tend to occur at greater depth in higher-velocity material, thus yielding this contrast in apparent source characteristics. The second term implies that explosions detonated in high–Poisson ratio material will have relatively larger $m_b - M_S$ offsets as well.

An obvious phenomenon related to mechanism is the type of wave generated. Barring tectonic release and collapse, explosions do not directly generate shear waves or, at longer periods, Love waves. Hence explosions will generally be depleted in such energy relative to earthquakes, particularly small explosions ($m_b \leqq 4.5$) that generally do not ex-

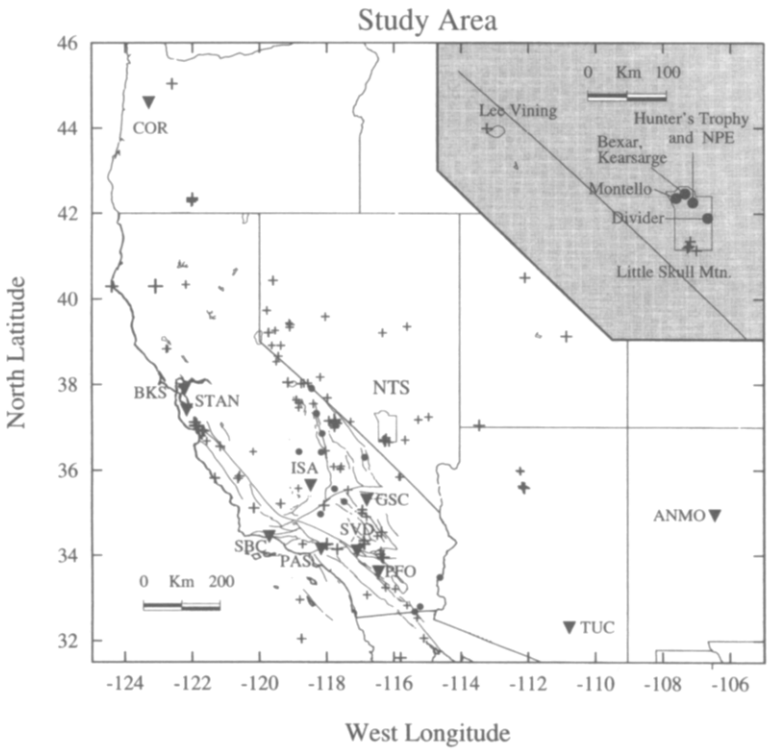

Figure 2. Map showing the stations (upside-down triangles), earthquakes (crosses), and small ($M_L < 3.0$) chemical blasts that, along with NTS explosions, make up the data used to evaluate the energy discriminants. NTS's boundary is outlined. Events used for waveform comparisons in this article are shown in the shaded enlarged inset with NTS explosions denoted by filled circles.

Table 1
Events with Waveforms Shown in This Study

Event	Date	Time	Lat.	Lon.	Depth	m_b
Lee Vining	90/10/24	6:15:20	38.05	−119.16	8.3	5.4
Little Skull Mountain	92/ 6/29	10:14:22	36.68	−116.28	11.0	5.6
L.S.M. Aftershock 1	92/ 6/29	10:31:02	36.70	−116.25	5.0	4.3
L.S.M. Aftershock 2	92/ 6/29	10:40:50	36.76	−116.24	5.0	3.8
L.S.M. Aftershock 3	93/ 5/30	15:21:03	36.65	−116.15	2.0	4.0
Kearsarge (P)	88/ 8/17	17:00:00	37.29	−116.31	0.6	5.5
Montello (P)	91/ 4/16	15:30:00	37.25	−116.44	0.6	5.4
Divider (Y)	92/ 9/23	15:04:00	37.02	−115.99	0.4	4.4
Hunter's Trophy (R)	92/ 9/18	17:00:00	37.21	−116.21	0.4	4.4
NPE (R)	93/ 9/22	7:01:00	37.20	−116.21	0.3	4.1

hibit significant tectonic release. Earthquakes commonly have prominent Love waves down to $m_b = 3.5$, and so in this respect (the *SH*-wave field), small earthquake and explosion long-period source spectra are significantly different. Of course there will be exceptions to this for particular fault orientations and source-receiver geometries.

Spall effects may also be a cause of the observed short-period ($0.15 < f < 2.0$ Hz) enrichment of explosion source spectra relative to that of earthquakes. Theoretical results (Day and McLaughlin, 1991) and various observational studies (Viecelli, 1973; Stump, 1985; Taylor and Randall, 1989) conclude that spallation can be a significant contributor to short-period energy, while Day *et al.* (1983) and Patton (1988) find no appreciable spall energy at periods greater than 8 sec.

As with all body-wave/surface-wave discriminants, the limiting measurement is that of the surface-wave amplitude. Lieberman and Pomeroy (1969) found the surface-wave detection level for earthquakes to be $m_b > 4.3$ and for explosions to be $m_b > 4.8$ for far-regional distances ($d \geqq 1000$ km) but found that the two populations converged below $m_b = 5.0$ for discrimination purposes. Below these threshold levels, the teleseismic surface-wave signals are within the noise level, and analogous discriminants using regional phases must be employed. Evernden *et al.* (1971), Lambert and Alexander (1971), and Peppin and McEvilly (1974) found that they could distinguish between earthquakes and explosions on the basis of the amplitude ratio of regional P_n to Airy-phase Rayleigh waves. The latter study found separation by source type for events down to magnitude (M_L) 3.6 for explosions and 3.3 for earthquakes. Taylor *et al.* (1989) found similar long-period measurement threshold

levels ($m_{b(Pn)} > 3.8$ for explosions and $m_{b(Pn)} > 3.3$ for earthquakes) in this region. The western United States is known to be a region of low Q (Patton and Taylor, 1984). It is expected that regions with high Q will have lower magnitude thresholds for measuring surface waves.

Woods *et al.* (1993) employed local magnitude (M_L) and seismic moment (M_0) as regional analogs to m_b and M_S measurements, respectively, and found that explosion and earthquake populations separate at all observed magnitude ranges. Patton and Walter (1993) obtained similar results using $m_{b(Pn)}$ as the short-period measurement and M_0 as the long-period measurement. Moment-tensor estimates, however, require reasonably accurate Green's functions (Zhao and Helmberger, 1994; Thio and Kanamori, 1995). At low magnitudes, moment estimates are susceptible to noise effects, although this problem can be minimized using phase-matched filtering (Herrin and Goforth, 1977). Such moment-calculating procedures are, however, fairly involved and would be difficult to implement for an automated monitoring system. Moment-tensor solutions assume an *a priori* source type (double-couple or isotropic source) that make it a less-than-ideal discrimination parameter. Stevens and McLaughlin (1988) approached this problem by treating all events as explosions; however, the events did not separate by source type below $m_b = 5$, and explosions below this magnitude did not have observable surface waves, and maximum likelihood moments were determined for them from their noise level. Even simple low-frequency spectral level methods (Vidal and Munguia, 1991) require estimates of source media properties for accurate moment calculations, and unless there are multiple observations at different azimuths, radiation pattern effects will not be adequately accounted for.

Taylor *et al.* (1989) investigated a number of regional discriminants involving long-period measurements: m_b versus M_S and m_b versus long-period surface-wave energy density and found both to be effective at separating explosions from earthquakes. However, these methods still require path calibration, and the energy density method used is even more susceptible to signal-to-noise level (SNL) thresholds than peak amplitudes or magnitude ratio measurements.

In this article, we use a more empirical approach to the SP:LP discrimination problem. As such, it avoids the problems noted above for moment calculation techniques in that it requires no waveform modeling, and all events are processed in the same fashion. The analysis is simple and performed in the time domain, so that it would be very easy to implement operationally. Further, unlike other methods discussed, this one utilizes all three longperiod components, so that the long-period measurements are less susceptible to radiation pattern effects; i.e., should an observation for an earthquake be at a Rayleigh-wave node, there should still be appreciable Love-wave signal. Also, as mentioned before, incorporating Love-wave measurements should enhance the contrast in waveform spectral content between earthquakes and explosions because of the fundamental difference in source radiation; i.e., explosions do not generate Love waves unless accompanied by tectonic release.

The E_{spP_Z}:E_{spS_Z} ratio, the other discrimination criterion studied, is essentially a measure of *P/Lg*, a review of which is given in Pomeroy *et al.* (1982). On the basis of previous work, they strongly suggest that the ratio of *P* to *Lg* is not a reliable discriminant, although explosions generally do have higher values than do earthquakes. Murphy and Bennett (1982) come to the same conclusion using amplitude ratios and a data set consisting of NTS explosions and nearby earthquakes recorded at TFO. However, they only address smaller explosions, thus limiting their data set to Rainier and Yucca shots, for which strong near-source scattering can complicate the spectra of phases of interest as is discussed later in this article.

With the advent of broadband digital stations coming on-line in the late 1980s, a new series of studies have been conducted. In their study of various regional discriminants applied to LLNL data, Taylor *et al.* (1989) found that network-averaged values of peak *P/Lg* ratios yielded misclassification rates between 30 and 50% but noted that these phases did have the lowest magnitude thresholds and thus had the most observations. Baumgardt and Young (1990) found that for regional NORESS data, both P_n/S_n and P_n/Lg amplitude ratios consistently separated mine blasts and earthquakes. Lynnes *et al.* (1990), in another study of NTS explosions and regional earthquakes (recorded at JAS), found that the spectral amplitude ratio of P_g/Lg in the 2- to 4-Hz range was fairly successful at differentiating events but performed more poorly at lower frequencies. Above this bandwidth, signal-to-noise ratio (SNR) problems resulted. Further, they noted that the ratios for the explosions increased with magnitude and depth. Kim *et al.* (1993) found that *P/Lg* spectral ratios measured in a multi-variate scheme between 5 and 25 Hz were quite successful at distinguishing earthquakes from quarry blasts in New England.

Walter *et al.* (1995) extend the study of Taylor *et al.* (1989) by applying P_n/Lg and P_g/Lg amplitude ratios to a comprehensive data set consisting of explosions from the three testing subregions and earthquakes lying within or very near the test site, thus minimizing path effects. However, only two LLNL stations were used. They found that network-averaged P_n/Lg amplitude ratios (6 to 8 Hz) plotted versus magnitude [M_L(coda)] fairly well separated events above M_L (coda) = 3.5, barring one significant outlying shallow earthquake. At lower magnitudes, the two populations begin to merge. P_g/Lg results are similar, but there is more overlap in the two populations.

We apply our version of this discriminant, which is essentially a measure of the root mean square P_z/S_z wave-train particle velocity ratio, to TERRAscope and other western U.S. IRIS stations. Besides giving the results for the aggregate data set, we will show results for eight individual stations—a significantly larger number of stations than in these aforementioned studies. Again, we take a simple, empirical

approach to the problem and do not attempt to introduce receiver or path corrections.

Method

The source properties that we want to quantify are the short-period ($f \geqq 1.0$ Hz) *P*-wave and long-period ($0.167 \leqq f \leqq 0.05$ Hz) surface-wave energy levels, the ratio of which is used as the discrimination criterion. The short-period bandpass is similar to that used to measure teleseismic *P*-wave amplitudes for the m_b:M_S discriminant. The long-period bandpass represents the predominant frequency range of the fundamental-mode Airy phase at regional distances (Alewine, 1972). This short-period versus long-period energy ratio (E_{spPz}:E_{lp-3}) is defined as

$$E_{spPz}:E_{lp-3} = \frac{\int_{tP_n}^{tS_n} v_{sp}(t)^2 dt}{\sum_{i=1}^{3} \int_{t_1}^{t_2} v_{lp}(t)^2 dt}, \quad (1)$$

with the summation being for the three components and t_i denoting the windowing times determined from travel path length and the wave train of interest: t_{P_n} corresponds to the time before the onset of the *P*-wave onset and t_{S_n} the time prior to the *S*-wave onset—usually 5 to 10 sec beforehand, and t_1 and t_2 bracket the time window of the fundamental Rayleigh and Love waves. The short-period and long-period ground velocities are respectively v_{sp} and v_{lp}. The velocities are squared in order to obtain units of energy; the term for the unit mass of the particle of motion cancel out in the numerator and denominator. Essentially we are quantifying the energy in specific wave trains and bandwidths. Kanamori *et al.* (1993) used the same methodology to quantify the energy in the broadband *S* wave train as a regional measure of energy magnitude.

Summation of the three long-period components is done in order to account for both the Rayleigh- and Love-wave energy as discussed above. Should only the vertical-component data be available, this discriminant measure would be no more effective than the conventional regional m_b:M_S method. Should one component be down, an ersatz modification can be made to the method in order to obtain useful information from the remaining components: The two-component sum can be multiplied by a factor of 1.5, thereby assuming the energy on the missing component to be an average of the other two components. However, if the tangential component primarily comprises this missing component, one is again confronted with the situation of only measuring the *P-SV* system, thus being potentially susceptible to radiation pattern effects of earthquakes, and it would be best to throw out the observation.

In developing this discrimination criterion, we found that the long-period energy is best measured by applying a narrow bandpass filter (between 7 and 20 sec) to isolate the regional fundamental-mode surface wave. Because explosions are relatively shallow sources, they generate large *Rg* waves as well as scattered, large-amplitude, surface-wave coda with periods of 6 sec or less. This feature is observed in Figure 1. Note that on both the broadband displacement and PE traces for Kearsarge, there is sizable Rayleigh-wave coda after the Airy phase. In comparison, the long-period Lee Vining and Little Skull Mountain earthquake records show very little or no Rayleigh-wave coda; rather, they each primarily display a fundamental-mode Airy phase and some earlier-arriving higher-mode waves.

These codalike surface waves generated by NTS events are believed to be generated preferentially by shallow sources. Kafka (1990) found a similar correspondence between shallow events and coda energy in a study of New England earthquakes and quarry blasts. Mayeda and Walter (1996) found that shallow earthquakes ($D \leqq 5$ km), collapses, and explosions show anomalous spectral peaking in the 0.2- to 0.4-Hz frequency range of coda waves relative to normal-depth earthquakes. They suggest that this may be related to the strongly depth-dependent phase *Rg* that scatters into the coda. Filtering out the short-period coda surface waves improves this discriminant as such energy would increase the measured long-period energy level, causing any shallow source to appear to be an earthquake.

As with other SP:LP discriminants, the limiting measurement is still the long-period signal. For this study, observations with SNLs as low as unity are used. More accurate estimates of the long-period signal can be made if the effect of noise is removed. One method to improve the long-period signal measure at these lower magnitude thresholds is to remove the effects of ambient noise by taking a portion of the integrated energy outside the arrival window of the transient signal and normalizing this sum (E_N) to the length of the time window of interest and obtaining a modified integrated energy for the signal, E_S':

$$E_S' = E_S \times \frac{E_S}{(E_S + E_N)}, \quad (2)$$

for which E_S' would near E_S for high SNR records and $E_S/2$ for the case $E_N = E_S$. However, this technique was not applied in this study.

The short-period *P*:*S* ratio (E_{spPz}:E_{spSz}) is defined similarly to (1), except the denominator is replaced by the integrated short-period vertical-component energy in the *S/Lg* wave train. Using these short-period phases, the SNR only becomes an issue for $M_L \leqq 3.1$ events.

Data Analysis and Results

Broadband, regional recordings of 131 earthquakes in western North America and 32 NTS underground explosions occurring between 1988 and 1994, and having $M_L \geqq 3.5$, comprise the data set. The data come from the TERRAscope

array as well as other IRIS dial-up stations, with the more recent events having better station coverage. Altogether there are 107 event-station pairs for explosions and 650 for earthquakes. Figure 2 displays the study area and events used in this study. This region is unique in that there is a large amount of seismicity, both natural and man-made, which is well recorded by various broadband networks.

All data were processed in the same fashion. The analysis process described above is quite simple to automate, and so as a first run, all events were done this way. The time interval chosen was determined from the distance-velocity relationship:

$$(r/v_1) - T_0 \leqq T_{\text{window}} \leqq (r/v_2) + T_0, \qquad (3)$$

where r is the path distance, v_1 and v_2 are the maximum and minimum wave-train velocities, respectively, and T_0 is an additional margin of time. After some experimentation, it was found that most suitable velocities for windowing the short-period P wave train were $v_1 = 7.9$ and $v_2 = 4.7$, and for the long-period surface wave and short-period S wave (Lg) trains $v_1 = 4.6$ and $v_2 = 2.5$ best windowed these phases. The windows were chosen to include the onset and the majority (roughly 85% or more) of the wave train of interest. $T_0 = 5$ sec for both cases.

Inspection of the energy curves indicates that high SNR events have sharp jumps in their energy curves. Primarily, the time windows were only set up so as to automatically process a large number events, i.e., to make sure that the time window encompasses the entire wave train of interest. However, for the most consistent measurements, it is best to use as narrow a time window as possible—particularly for low SNR events, for which cases the integrated energy is primarily a function of window length.

We now provide examples of observed waveforms, their respective integrated energy curves, and the time windows used for the energy measurements for the closest four stations: GSC, ISA, PAS, and PFO. They are for a suite of typical regional events—both explosions from the three NTS subregions and for earthquakes near NTS (from the Little Skull Mountain sequence). A catalog that lists these events is given in Table 1. Their locations are shown in the enlarged inset of Figure 2.

Figure 3 displays vertical-component velocity records of NTS shots recorded at GSC ($160 < r < 220$ km). At this station, the long-period fundamental-mode Rayleigh-wave energy is evident for all events, although in the case of Hunter's Trophy, the Rayleigh wave train is within the noise level. We will address this problem later. In the short-period band, the explosions exhibit waveform characteristics that are site specific in that they are observed to be self-similar to other events from the same test site subregion. This holds true for all TERRAscope records gathered to date; Pahute Mesa events tend to generate very little S-wave (or Lg) energy, while Yucca Flat events have strong S waves that are often larger than the P waves, and Rainier shots are intermediate in character with shear-wave arrivals that rival the peak P_g wave in amplitude. The characterizations are based on visual inspection of the entire waveform database.

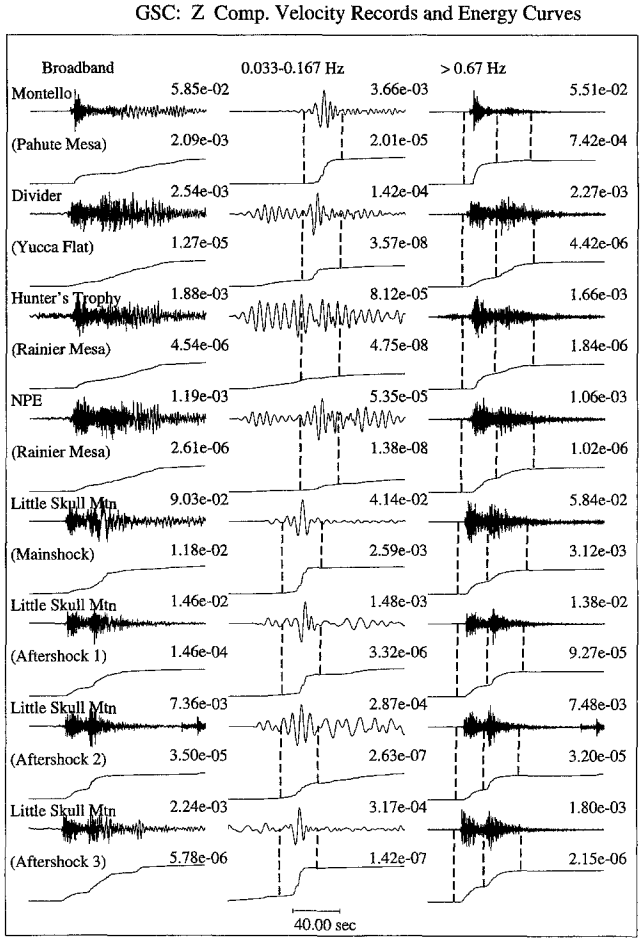

Figure 3. A comparison of vertical-component velocity records for NTS explosions and Little Skull Mountain sequence earthquakes recorded at GSC. The first (left) column is the broadband play out, followed by the long-period, filtered record in the second (middle) column and the short-period, filtered record in the third (right) column. Directly beneath each seismogram is its associated integrated energy curve. For the long-period and short-period play outs, the time windows used to measure the integrated energy are denoted by the vertical dashed lines. Each event's identification (and in the case of explosions, also the test subregion) is to the left of the records. Peak ground velocity amplitudes (cm/sec) and total integrated energy (cm^2/sec^2) are given above each trace.

It should also be noted that the short-period waveforms for the Non-Proliferation Experiment (NPE) (Denny and Zucca, 1993) and the other Rainier shot, Hunters' Trophy, are very similar. In all cases, the S wave train for the explosions does not have a sharp onset but, rather, is dispersive. This behavior also is spread out in the energy curves. The short-period integrated energy curve for Pahute resembles a step function produced by the very prominent P-wave ar-

rival. The Yucca curve is more ramplike with a second prominent ramp for the *S* wave. Again, the Rainier events are intermediate in character. The earthquakes all have their most pronounced jump in energy at the *S*-wave arrival.

Also note that in the broadband traces, the $T \leqq 7$-sec dispersed *Rg* and short-period surface-wave coda are the predominant phases on the Yucca Flat and Rainier Mesa events and that the Pahute shot also generates considerable energy of this sort, whereas the earthquakes exhibit little such energy with the exception of aftershock 3, the bottom record. This event is actually from Rock Valley, a zone of very shallow seismicity ($1 \leqq D \leqq 3$ km) (Smith and Brune, 1993). Walter *et al.* (1995) found this sequence to exhibit anomalous behavior characteristic of explosions using their discriminants. This shallow of an earthquake is expected to generate large *Rg* waves (Kafka, 1990). Note that this event did fall within the earthquake population with respect to the SP:LP discriminant.

In making comparisons between events, it should be noted that the Pahute shot is larger than the others, so that it has a higher SNR. There are no distinguishing features on the long-period recordings among the three test subregions or for the NPE explosion.

Figure 4 plots the waveforms for the same suite of events recorded at ISA ($230 < r < 270$ km). Once again, the explosions tend to exhibit more *Rg* energy than do the earthquakes with the exception of aftershock 3, which is thought to be shallower than the other earthquakes. In the short-period passband, the explosions exhibit very little *Lg* energy, even for the Yucca shot, thus yielding steplike energy curves at the *P*-wave arrival, but with no significant jump at the *S*-wave arrival. We attribute this lack of *Lg* to blockage caused by propagation across the Sierra Nevada block and Death Valley; as at the other stations, there is always a prominent *S* wave or *Lg* phase for Yucca shots. This observation becomes more apparent after viewing the PAS and PFO records. The earthquakes all have sharp, prominent *S*-wave arrivals that are due to direct body waves as well as to trapped shallow, crustal, *Lg* energy.

For the long-period passband (middle column), the SNR becomes an issue. The two Rainier events' (the 3rd and 4th rows of seismograms) surface waves have SNRs approaching unity, as are those for the bottom two earthquakes. The integrated energy for these low SNR records correspondingly is primarily a function of the window length, as the noise dominates the contributions to the curve, showing only small rises at best at the surface-wave arrival. E_{spPz}:E_{lp-3} measurements for such cases should be considered ratio minimums, for the actual long-period surface signal contribution is less than the apparent signal. Consequently, the discriminant was applied to records for all events with $M_L > 3.5$, in part to ascertain its performance at its measuring threshold. Constraining the time window used to be as narrow as possible also mitigates this problem somewhat. We did reapply narrower time windows (than those described earlier,

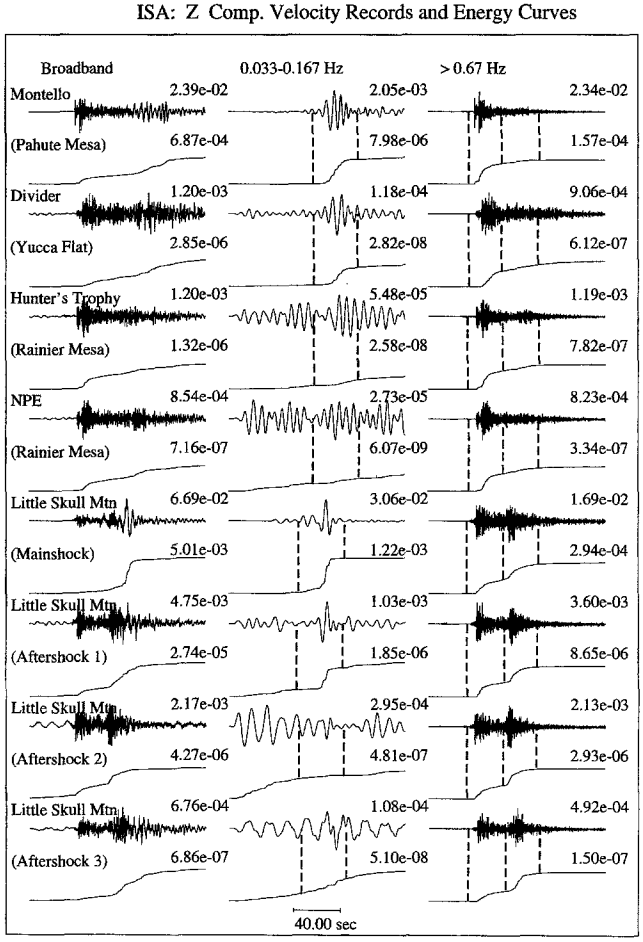

Figure 4. A comparison of vertical-component velocity records for ISA.

which were used for the entire data set) to calculate the long-period energy for individual low SNR records.

These recordings are at fairly near distances ($160 < r < 270$ km), so that propagation effects are minimal. An extension of these comparisons to the more distant ($330 < r < 400$ km) stations PAS and PFO is given in Figures 5 and 6, respectively.

Again, the explosions exhibit more late-arriving energy due to the *Rg* phase and scattered phases than do the earthquakes, the exception being aftershock 3 or the Rock Valley earthquake. The late-arriving energy seen in the aftershock 2 records is due to a separate local event that can be seen more clearly in the short-period play out. At these distances, the long-period surface-wave signals begin to merge with the seismic noise; however, these records suggest that the long-period portion of the source spectra does not discontinuously drop off but rather decreases below the SNR of the recording site. For events with comparable long-period amplitude events, the short-period records of the explosions have larger amplitudes than the earthquakes, also supporting the E_{spPz}:E_{lp-3} discrimination criterion.

At these more distant stations, Pahute recordings still

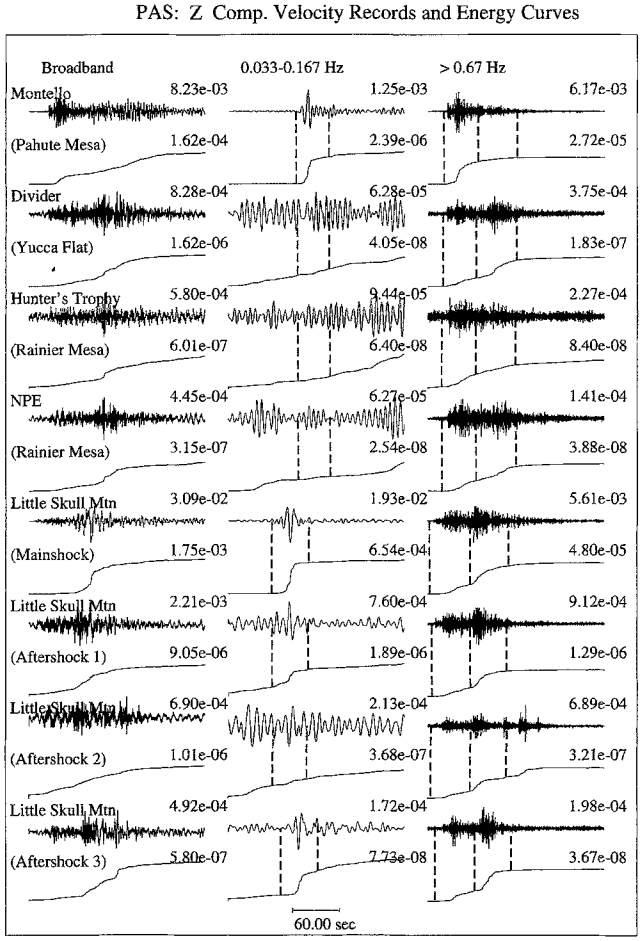

Figure 5. A comparison of vertical-component velocity records for PAS.

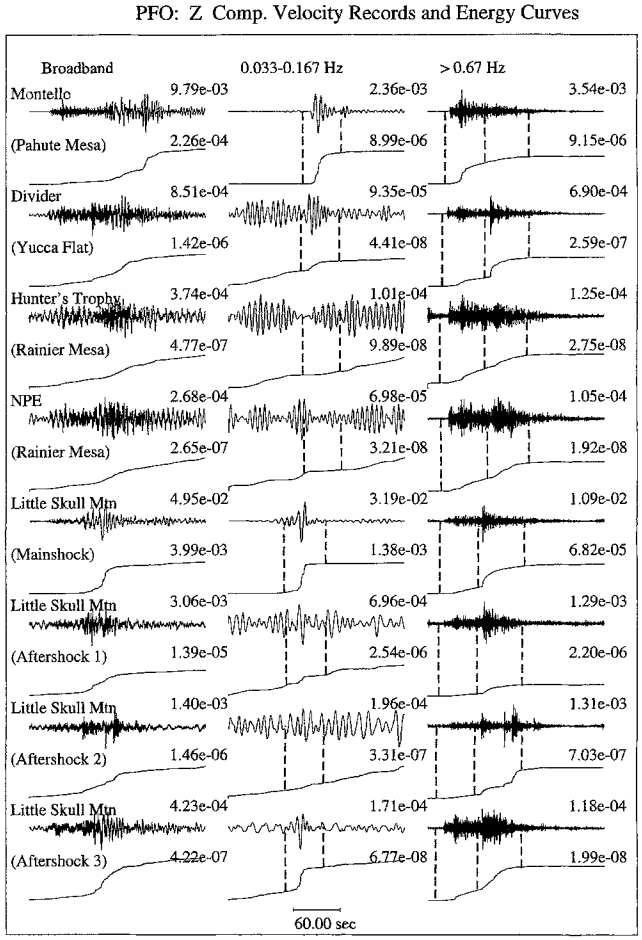

Figure 6. A comparison of vertical-component velocity records for PFO.

retain their strong, prominent *P*-wave arrivals, with only small amounts of energy in the expected shear-wave time window, whereas the other explosions more closely resemble earthquake waveforms in that they have comparable amounts of *S*-wave energy. Divider, the Yucca event, in fact has larger-amplitude *S* waves than *P* waves, and its *S*-wave energy is greater than the *P*-wave energy as well. One can see this visually in the integrated energy curves. Still, for earthquakes, the *S* wave-train arrival is more distinct and generally larger than the *P*-wave arrival. This general observation does not hold for the case of the PFO recording of the explosion Divider, however, which has a very sharp *S*-wave arrival more than twice as large as anything in the *P* wave train and looks very much like a typical short-period earthquake record. It should be noted that these waveforms for the NTS events tend to be very characteristic of each subregion; for instance, this sharp *S* wave is observed at all PFO recordings of Yucca shots.

This increase in *S*-wave/*Lg* energy in the more distant explosion records is believed to be due to propagational scattering effects of already converted *P* to *SV* phases. Such energy is absent from most recordings of Pahute events, whereas there is evidence of significant conversion to *S*-wave energy for Rainier and Yucca recordings. We have examined all available explosion records and found that in the short-period bandwidth, all explosions recorded at any one station and from one specific NTS subsite are quite similar.

Visual inspection of each station-event pair energy curve was performed in order to ensure that the time windows encompassed the appropriate wave trains for the energy measurements. An estimated 10% or fewer of the records needed their time windows modified. For the purposes of an operational monitoring system, a regionalized velocity map could be implemented as part of a calibration process in order to fully automate such an analysis.

A plot of the ratio of E_{spPz}:E_{lp-3} versus distance for all events above $M_L = 3.5$ is displayed in Figure 7a. The explosions tend to have higher value ratios than do the earthquakes at all distances. Although there is not complete separation of the two populations, overlap is small, with 8% of the earthquakes and 5% of the explosions being misclassified. It appears that separation is greatest at longer distances ($r \geqq 900$ km) and least at distances less than 400 km. This

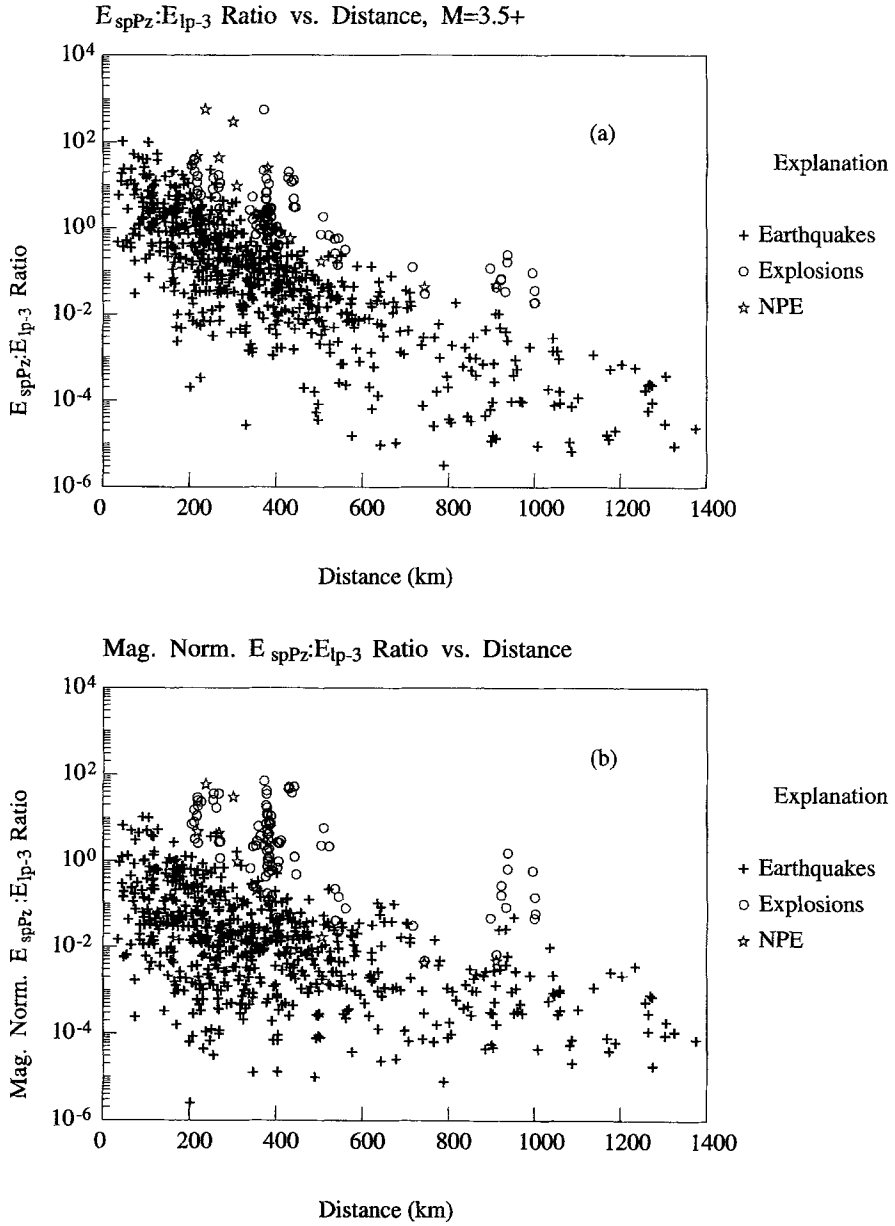

Figure 7. (a) Plot of the short-period:long-period energy ratio (E_{spPz}/E_{lp-3}) versus distance for $M_L = 3.5+$ events. Each datum point represents one source-receiver pair. Earthquakes are represented by crosses, and the NTS explosion is represented by circles. The NPE shot is denoted by stars. (b) Plot of magnitude normalized energy ratio versus distance for the same data set.

effect may have to do with the sampling populations, however. Earthquake datum points at larger distances are usually from larger events ($M_L \geqq 5.0$), for which the difference in relative short-period to long-period energy levels between earthquakes and explosions is already firmly established.

There is significantly more scatter in the earthquake population than in the explosion population. Several factors are believed to be responsible for this effect: (1) there is large azimuthal variation for earthquakes due to mechanism, whereas explosions are predominantly isotropic sources; (2) paths are more varied for earthquakes; and (3) explosions have a extremely regular source depth of less than 1 km, whereas earthquakes within this geographic region range between 1.0 and 15 km in depth, with most earthquakes being between 5 and 12 km (Zhu and Helmberger, 1996). Another quality of the earthquake energy ratio data is that population outliers are skewed, with the upper boundary having an abrupt end, while the lower boundary is more diffuse. It is interesting to note that the energy ratios for the NPE chemical explosion are similar in value to those of the nuclear ones.

Often, discriminant parameters are plotted versus magnitude in order to remove source scaling effects, i.e., Mayeda

and Walter (1996) and Taylor *et al.* (1989). As we have not removed propagation effects, which are significant, it is not possible to compare directly the energy ratio values to magnitude. However, we did investigate the effect of normalizing the energy ratio values with respect to magnitude. From our E_{spPz}:E_{lp-3} observations, it was evident that the larger events (particularly earthquakes) usually had lower energy ratios, thus we applied a normalization of the following form:

$$E_{spPz}:E'_{lp-3} = E_{spPz}:E_{lp-3} \times 10^{(m-m0)}, \qquad (4)$$

where m is the event's magnitude (m_b or an equivalent scale) and m_0 is a reference magnitude we chose as 5, as it is around the median magnitude of events being analyzed. Figure 7b plots this normalized energy ratio versus distance. Far better separation with respect to event type is obtained at the shorter distances, while the more distant datum points show no improvement in separation. This effect may be due to the signal level of the records. At greater distances, most of the available explosion data are for small events ($M \leqq 4.5$), whereas larger events ($M \geqq 5$) comprise most of the earthquake data. The larger events' energy ratios will increase more than the smaller ones when normalized, so consequently in this case the normalized earthquake energy ratios will rise relative to those of the lower magnitude explosions.

How well the E_{spPz}:E_{lp-3} discriminant performs at individual stations is of interest in order to ascertain whether or not there is significant station bias in these measurements. Also, individual station performance is an important aspect of operational considerations, since sparse station coverage and low magnitude threshold-monitoring requirements will often require that identification be made with single-station observations.

The data recorded at the four longest-running TERRAscope stations are plotted in Figures 8a through 8d. These four stations (GSC, ISA, PAS, and PFO) are the closest stations to NTS, and they have recorded the largest number of events. As in the complete data set plot, there is some overlap in earthquake and explosion populations, but all explosions still plot higher than most earthquakes. Also note that there are not significant differences between the test subregions, but rather all explosion datum points tend to cluster. The largest scatter in explosion values is for PAS, which also had the most data. However, the scatter shows no correlation with test area. As for station site effects, these four stations all have earthquakes in the same distance range, and their energy ratios plot in the same range, implying that receiver effects are relatively small.

Plots of the E_{spPz}:E_{lp-3} ratio for stations ANMO, TUC, COR, and BKS (along with STAN) are displayed in Figures 9a through 9d, respectively. No station-related patterns are found, implying that receiver effects are fairly insignificant.

Besides comparing integrated energy ratios, SP:LP peak ground velocity amplitude ratios were also determined for all data, the results of which are shown in Figure 10. The

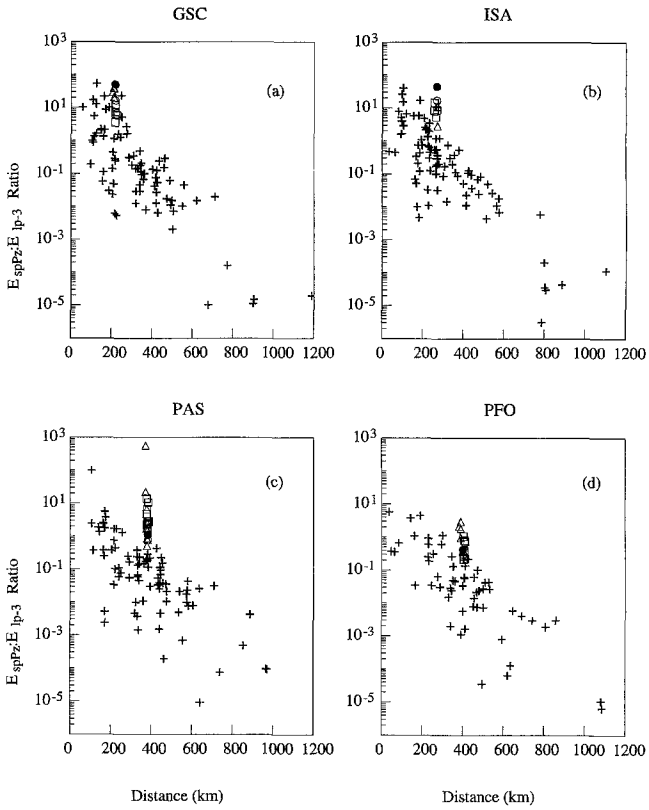

Figure 8. Plots of E_{spPz}/E_{lp-3} versus distance for the individual stations: (a) GSC, (b) ISA, (c) PAS, and (d) PFO. Crosses denote earthquakes. NTS events are separated by subsite: Yucca Flat (triangles), Pahute Mesa (squares), and Rainier Mesa (circles). The NPE is denoted by solid circles.

long-period value is the sum of the three-component peak values. This method separates the two populations about as well as the integrated energy ratio method. There are two advantages to using peak amplitude measurements. As peak amplitudes are used, better measurements can be made of very low SNR records, and analog data (such as historical analog seismograms) can be used as well.

As mentioned earlier, we also examined the potential of a short-period P to S (or Lg) discriminant (E_{spPz}:E_{spSz}). This measure is potentially useful for smaller events that radiate little or no observable long-period surface-wave energy. This measurement is quantified similarly to E_{spPz}:E_{lp-3}, except that the denominator now is an integral of the short-period squared velocity over the S-wave (including Lg) time window. The velocities used to window the data are 7.9 and 4.7 km/sec for the *Pnl* wave train, and 4.6 and 2.5 km/sec for the *S*/*Lg* wave train. As this method only requires short-period data, the measuring threshold is lowered to $M_L \geqq 3.0$. At closer distances ($r \leqq 200$ km), this threshold can be extended to even lower magnitudes.

E_{spPz}:E_{spSz} ratios for the data set, which includes all the events previously studied as well as others collected in the $3.0 \leqq M_L \leqq 3.5$ range, are displayed in Figure 11. At this

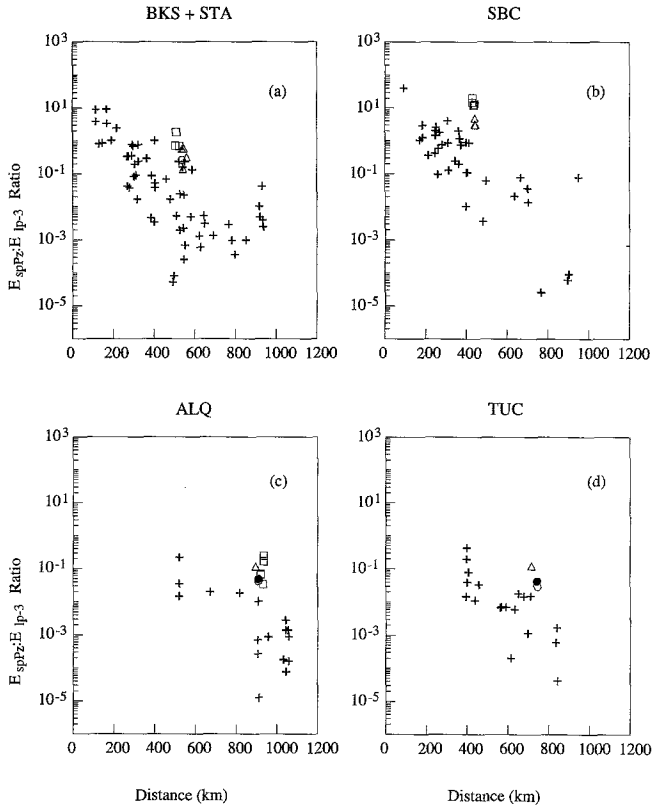

Figure 9. Plots of E_{spPz}/E_{lp-3} versus distance for the individual stations: (a) BKS and STA, (b) SBC, (c) ALQ, and (d) TUC.

threshold, it was possible to include several quarry blasts from southern California as well as shots from the Southern Sierra Continental Dynamics (SSCD) Project (Fliedner and Ruppert, 1994) to the data set. These shots are marked by squares in the figure. The separation of populations is poorer using this method, with overlap being estimated at 50%; however, the explosions population does, on average, have higher *P*:*S* energy ratios than does the earthquake population.

Several observations to note are that small chemical blasts do tend to have relatively high *P* to *S* energy ratios, while the larger NPE blast, on the other hand, yields relatively low energy ratios compared to nuclear explosions. However, at these short periods, receiver (as well as path) effects are likely to be significant. Visual comparisons of event waveforms at different stations provided examples of this. Some stations, such as BKS, PFO, SBC, and STAN, exhibited considerably more *S*-wave and *Lg* wave-train energy than other stations for the same events.

In an attempt to remove receiver effects, the E_{spPz}:E_{spSz} data for GSC, ISA, PAS, and PFO were sorted by station and plotted in Figures 12a through 12d, respectively. Binning by receiver yields some improvement in separating the populations; however, there is still considerable overlap between the earthquake and explosion populations. It is clear that the NTS subsites do display different trends, with Yucca and Rainier shots having more shear-wave energy than Pahute tests. This is particularly true for PAS, which has the largest number of observations. Again the NPE shot plots low relative to most of the nuclear explosions.

E_{spPz}:E_{spSz} ratios for the stations ANMO, TUC, COR, and BKS (along with STAN) are displayed in Figures 13a through 13d, respectively. Again, NTS explosions have been plotted by subregion. Similar separation of source types is obtained, with Pahute events having the highest E_{spPz}:E_{spSz} ratios.

Reviewing these short-period E_{spPz}:E_{spSz} plots in Figures 12 and 13, it is apparent that the energy ratio levels do vary somewhat between stations, thus suggesting station bias. This is not surprising since this ratio is a product of two short-period measurements that are susceptible to relatively small-scale wave-guide features. Thus, this discriminant should either be applied on an individual station basis or would require station corrections.

The E_{spPz}:E_{spSz} values also were normalized with respect to magnitude. This did not improve the separation between earthquakes and explosions as it had in the case of the E_{spPz}:E_{lp-3} experiments; however, it did increase the separation between explosions at Pahute and those at Yucca and Rainier. This result implies that near-source effects play a crucial part in the conversion of *P* or *Rg* energy to *S*-wave energy.

Other studies of short-period phase ratios (Taylor *et al.*, 1989; Lynnes *et al.*, 1990; Walter *et al.*, 1995) have found that spectral amplitude ratios are magnitude dependent. To examine this effect we plot the unmodified E_{spPz}:E_{spSz} values against M_L without correcting for distance. The results for the entire data set are shown in Figure 14; NTS events have been binned by subsite for plotting. Little or magnitude dependence is apparent for the earthquakes. Taken in aggregate, explosions appear to show some dependence between E_{spPz}:E_{spSz} and magnitude. However if the individual subsites are examined, no such dependence is observed. The Pahute events do have significantly higher E_{spPz}:E_{spSz} ratios than do the other two subsites, which quantifies our visual observations that Pahute events generate "clean" explosion records with a prominent *P* wave and little or no *S*/*Lg* wave train. However, as the Pahute shots are generally the largest from NTS, and consequently buried the deepest, this effect could also be due to depth and/or source medium.

Since we incorporate no receiver corrections, it is worthwhile to examine the discriminant at individual stations. Figure 15 plots this for the four closest and longest-running stations. No apparent magnitude dependence is observed for the E_{spPz}:E_{spSz} values, although as magnitude is also a function of shot site, it is difficult to clearly ascertain. Also, no better separation of earthquakes and explosions is achieved than when plotted versus distance (see Fig. 12 for comparison). Similar results were obtained for the other stations but are not plotted here.

Some studies of regional short-period discriminants have found better discrimination at higher frequencies (Kim and Richards, 1993; Walter *et al.*, 1995) whereas Taylor *et*

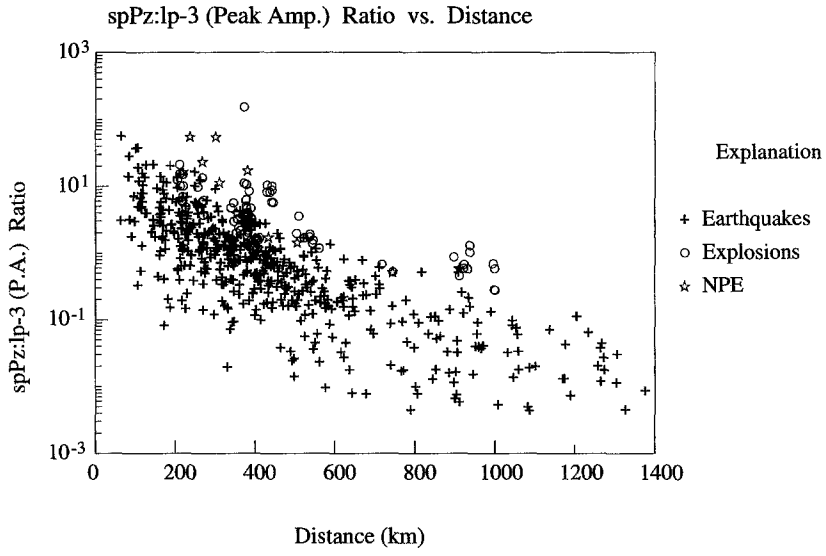

Figure 10. A short-period:long-period discriminant determined from the peak amplitude within the pertinent time window, as opposed to integrated energy (Fig. 7).

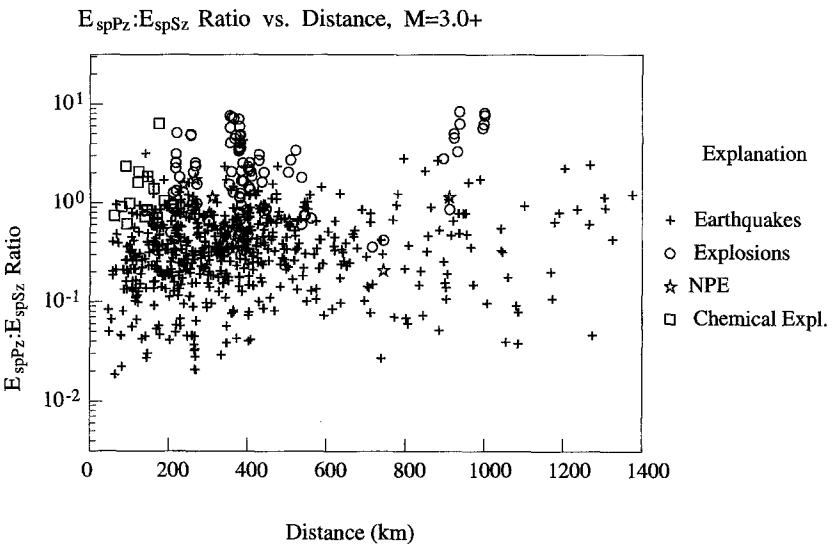

Figure 11. Plot of E_{spPz}/E_{spSz} versus distance for all events $M \geqq 3$ or greater. Crosses represent earthquakes, circles denote nuclear explosions, stars are for the NPE, and squares denote smaller chemical blasts.

al. (1989) found no such effect. Consequently, we also examined the effect of applying a higher-frequency band on the E_{spPz}:E_{spSz} ratio. Figure 16 compares E_{spPz}:E_{spSz} ratios for records convolved with a Wood–Anderson short-period (similar to high-passing at 1.0 Hz) instrument (open symbols) to those that have been further high-pass filtered at 4 Hz (filled symbols). The events used are those for which waveforms were shown in Figures 3 through 6. This subset of events was used in order to minimize path effects for this comparison. The effect of taking the *P*:*S* energy ratio to higher frequencies increases the ratio value in general but is greatest for the explosions. This result implies that explosions, compared to earthquakes, are relatively more deficient in *S*-wave (or *Lg*) energy at higher frequencies.

Discussion

There are several explanations for the observed difference in SP:LP spectral character between earthquakes and explosions. Source mechanism, no doubt, plays a significant role for earthquakes; however, this effect is highly variable, which the large scatter in the E_{spPz}:E_{spSz} earthquake population bears out.

The theoretical argument by Stevens and Day (1986) that source-medium properties are a significant factor in accounting for the off-set in $m_b - M_S$ between earthquakes and explosions is quite compelling, especially since earthquakes are almost always deeper than explosions and thereby have different source regimes. Shallow ($D > 5$ km) earthquakes, when they do happen, tend to be very low stress-drop events that are relatively enriched in long-period energy.

As for the source spectrum itself, earthquakes tend to be distributed sources with corresponding considerable rise times, as opposed to explosions that have relatively short rise times more aptly modeled as step-function point sources at long periods with an impulsive component (overshoot) at

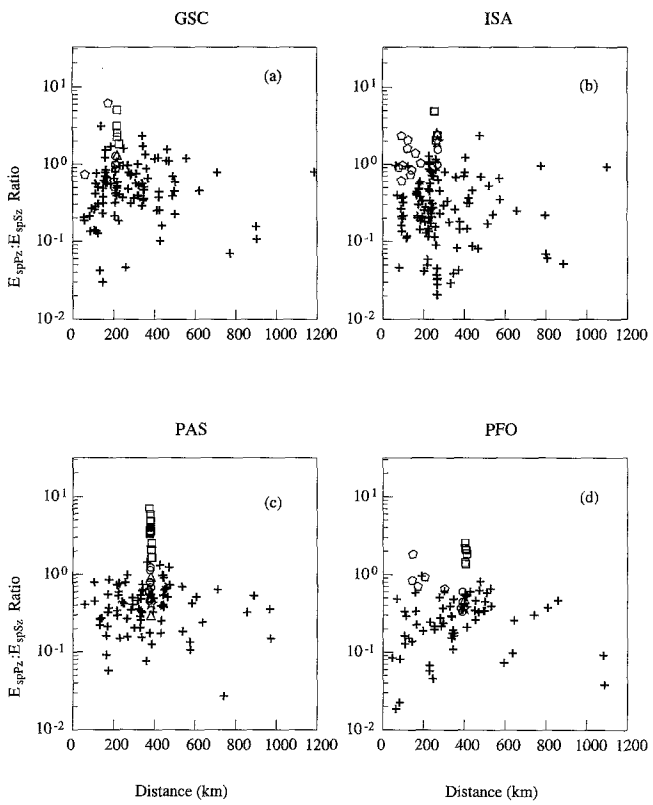

Figure 12. Plots of E_{spPz}/E_{spSz} versus distance for individual stations: (a) GSC, (b) ISA, (c) PAS, and (d) PFO. Crosses represent earthquakes. NTS events are sorted by subsite: Yucca Flat (circles), Pahute Mesa (squares), and Rainier Mesa (triangles). The NPE is denoted by stars. Smaller chemical explosions are denoted by pentagons.

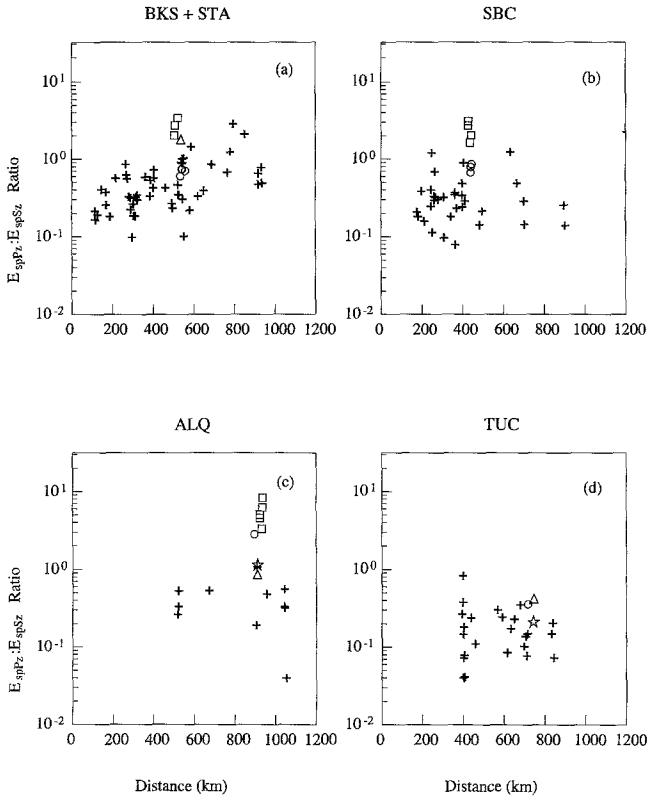

Figure 13. Plots of E_{spPz}/E_{spSz} versus distance for individual stations: (a) BKS and STA, (b) SBC, (c) ALQ, and (d) TUC. Crosses represent earthquakes. NTS events are plotted as separate symbol types for Yucca Flat (circles), Pahute Mesa (squares), and Rainier Mesa (triangles) shots; the NPE is denoted by stars.

shorter periods. Dreger and Helmberger (1991) showed that broadband seismograms from small local earthquakes ($4.0 < M_L < 5.0$) can be modeled as distributed finite sources rather than as point sources. Such distributed slip time functions will generally result in reduced short-period spectra relative to a point-source step moment. It is possible that even very small earthquakes ($M_L < 4$) behave similarly.

Consider the extreme case of an $M_L = 3.5$ earthquake for which the source radius is upward of 1 km (Peppin and McEvilly, 1974; Vidal and Munguia, 1991) and the rise time is a function of the shear velocity. The corner frequency of such an event is on the order of 1 or 2 Hz, following the method of Hanks and Wyss (1972). For a comparable magnitude explosion ($Y \sim 0.5$ kt), we obtain from the appropriate source-scaling curves (Denny and Johnson, 1991) a source radius less than a tenth this size and a corner frequency that is upward of 4 Hz. Further, the rise time is dependent on the compressional velocity. Thus even at these low magnitudes, differences in source spectrum should be observable on the TERRAscope and IRIS broadband systems that have a flat velocity response up to 7 Hz.

It seems reasonable that a combination of these factors is responsible for the difference in SP:LP energy level between earthquakes and explosions.

The reason for the poor performance of the E_{spPz}:E_{spSz} discriminant is that some explosions do exhibit strong *S* wave and *Lg* wave trains at short periods that yield low *P*/*S* energy ratio values. This effect is strongly source-site dependent. For TERRAscope observations, such shear-wave–rich explosions are without exception ones from Yucca and Rainier, with Yucca shots generally exhibiting the most shear-wave energy—often it is the most prominent arrival, as can be seen in Figures 3 through 6. Pahute, on the other hand, has more deterministic waveforms that are similar to Kazakh and Lop Nor explosion waveforms at similar distances (Woods and Saikia, 1994).

Near-source scattering effects are a likely explanation for these waveform differences, as the travel paths from the three NTS subsites to the TERRAscope stations are not drastically different. We hypothesize that the basin structure of Yucca Flat, the irregular cavity geometries due to tunneling (Zhao and Harkrider, 1992), and perhaps even the topography of Rainier Mesa are the causes of *P*- to *S*-wave scattering at these two sites.

The results of Walter *et al.* (1995) imply that the P_g/Lg

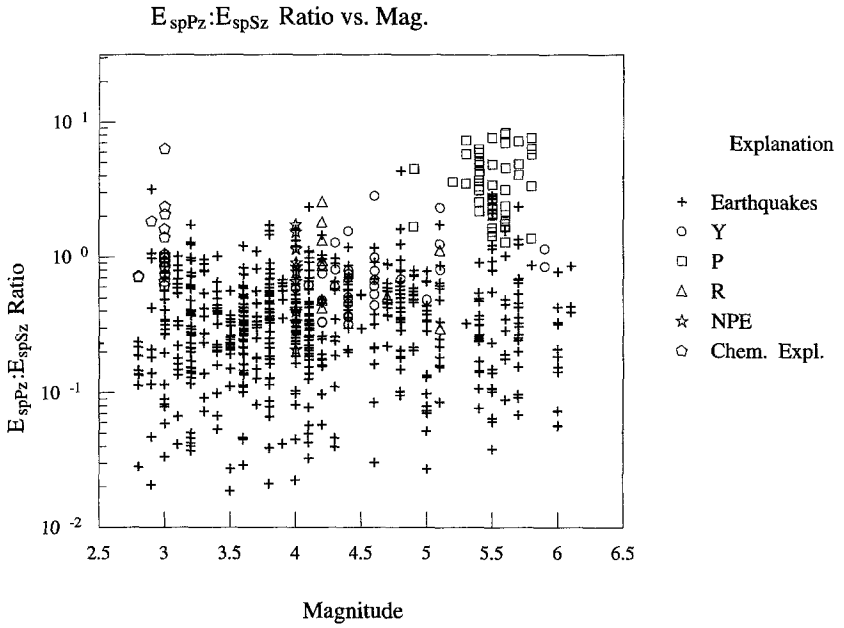

Figure 14. Plot of E_{spPz}/E_{spSz} versus magnitude. Crosses represent earthquakes. NTS events are plotted as separate symbol types for Yucca Flat (circles), Pahute Mesa (squares), and Rainier Mesa (triangles) shots. The NPE is denoted by stars. Smaller chemical explosions are denoted by pentagons.

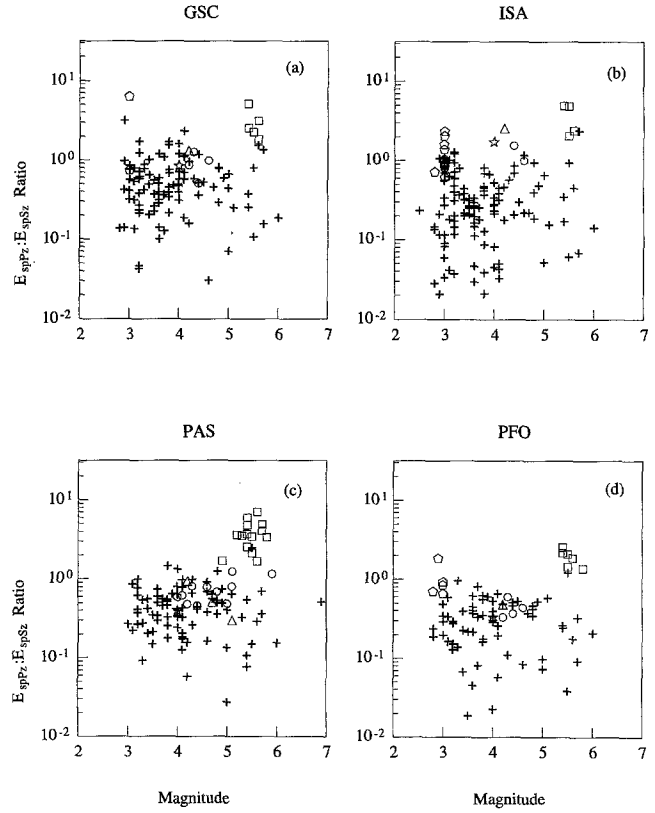

Figure 15. Plots of E_{spPz}/E_{spSz} versus magnitude for individual stations: (a) GSC, (b) ISA, (c) PAS, and (d) PFO. Crosses represent earthquakes. NTS events are plotted as separate symbol types for Yucca Flat (circles), Pahute Mesa (squares), and Rainier Mesa (triangles). The NPE is denoted by stars. Smaller chemical explosions are denoted by pentagons.

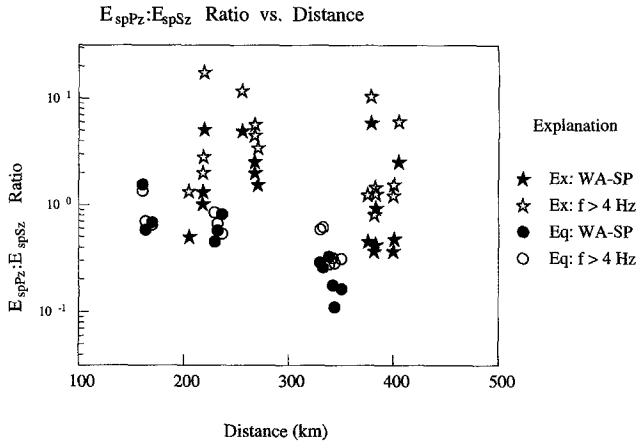

Figure 16. Plots of E_{spPz}/E_{spSz} versus distance for the events shown in Figures 3 through 6. Stars denote explosions, and circles represent earthquakes; solid symbols are for data convolved with a WA short-period instrument, and open symbols are for data that have been further high-pass filtered at 4 Hz.

ratio is dependent on source medium properties such as gas porosity, with shallow, high gas porosity shots being enriched in L_g. As the shallower shots all tend to be lower magnitude ones from Yucca Flat and Rainier Mesa, it is not clear whether source medium or near-source scattering is the predominant factor in these depressed explosion *P/Lg* ratios. The fact that Rainier shot sites are in a perched aquifer, which is corroborated by the low gas porosity values for Rainier events in the Walter *et al.* (1995) study, and yet these explosions still generate considerable *S/Lg* waves suggests

that source medium is not the sole or even primary contributor to such effects.

The fact that the character of the short-period *S/Lg* phases or wave trains is consistent for explosions from the same test area (Pahute, Yucca, or Rainier)—particularly when comparing records from one station—but varies between sites suggests that the short-period shear-wave energy is indeed due to near-source scattering effects such as conversion of *Rg* to *Lg* (Jih, 1995; Gupta *et al.* 1992; Jih and McLaughlin, 1988; Stead and Helmberger, 1988). We suspect that the alluvial basin structure of Yucca Flat and the tunnel shots in the side of a mountain at Rainier Mesa are responsible for these scattering effects. The NPE records closely resemble their nuclear shot counterpart at Rainier (Hunter's Trophy), further suggesting that the shear-wave energy level is predominantly due to near-source scattering effects.

This site-specific scattering for explosions may explain the results of some NTS discrimination studies, such as that of Murphy and Bennet (1982), which found poor separation on the basis of temporal *P/Lg* ratios. For their study, only explosions $m_b < 4.8$, and consequently only ones from Yucca and Rainier, were examined. We infer from our observations that strikingly different results would be yielded for a population of Pahute explosions.

The difference in character of short-period *S*-wave arrivals between GSC and PFO recordings of Yucca Flat explosions is curious because their great circle paths vary by less than 15°. However, this scattering of locally generated surface waves in the crustal wave guide can easily be a ray-parameter–dependent phenomenon that would allow complex patterns of wave packets to occur along the same azimuth, but at different distances, thus explaining the difference in *S*-wave arrivals between the two stations. As the prominent *S* arrival at PFO is only seen for Yucca events, it is not likely that the effect is caused by scattering along the path between GSC and PFO; otherwise, it would be expected to be seen for the other explosion source areas.

There is also considerable scatter among the earthquakes' short-period energy ratios. This is believed to be due to mechanism and propagation effects. As the vast majority (95%) of earthquakes studied occurred at depths greater than 5 km, assuming the seismic depth distribution and using the actual values from waveform modeling (Zhu and Helmberger, 1996) when possible, the crust is fairly homogeneous relative to that of the very shallow ($d < 1$ km) explosions, and scattering due to lateral variations near the source should be minimal in comparison. There were also several cases of earthquakes that had distinctly explosion-like waveform character with their *P* wave train being the most prominent phase.

Conclusions

We have examined the performance of two empirical seismic discriminants, which use regional broadband waveforms, by applying them to a large data set of regional explosion and earthquake records from the southwestern United States and Baja, Mexico. Both of these methods are based on energy integral measurements of particular wave trains in the time domain, which make them ideal to implement in an automated monitoring system.

The more promising discriminant is the E_{spPz}:E_{lp-3} energy ratio, for which explosions tend to exhibit higher values than earthquakes. This method can be considered a variation of the m_b:M_S discriminant applied to regional data. Although there is some overlap between the explosion and earthquake populations, the two source types do display significantly different overall trends with mean E_{spPz}:E_{lp-3} ratios at a given distance, being larger for explosions than for earthquakes. Misclassification rates are 8% and 5% for earthquakes and explosions, respectively. This discriminant then could be applied to screen out events that are easily identified, or as part of some multi-variate discriminant scheme.

Because this (E_{spPz}:E_{lp-3}) discriminant is applicable to a sparse broadband network, it is ideal to be implemented in a global monitoring scheme such as the IDC's International Monitoring System (IMS). For an active tectonic region, the threshold for the discriminant is $M_L = 3.5$ for earthquakes and $M_L = 4.0$ for explosions for epicentral distances up to 800 km, which correspond to teleseismic m_b threshold estimates [assuming the M_L:m_b relationship obtained by Chung and Bernreuter (1981)] of $m_b = 3.1$ and $m_b = 3.6$, respectively. As observations suggest that the long-period signals decrease below the SNL for smaller events rather than discontinuously dropping off, schemes to lower the long-period measuring threshold further, such as phase-matched filtering or the use of deep borehole instruments (with corresponding low noise levels) should be quite useful for this discriminant.

The E_{spPz}:E_{spSz} ratio does not separate the source types as well as the E_{spPz}:E_{lp-3} ratio, with an estimated 50% of the earthquake population overlapping with that of the explosions. Individual station performance is better with less than 30% overlap. From the time series and energy curves shown (Figs. 3 through 6), it is clear why the E_{spPz}:E_{spSz} energy ratio is not effective at identifying explosions from earthquakes. Near-source scattering and path effects can generate significant scattered shear-wave energy that masks the short-period *S*-wave character of a source; our observations indicate that near-source scattering is the primary factor. The E_{spPz}:E_{lp-3} ratio on the other hand is not as sensitive to such short-period effects, as the scattered energy shows up predominantly in the shear wave train and surface-wave coda ($T < 6$ sec) and least in the short-period P_{nl} and long-period ($T > 8$ sec) surface wave trains.

Better separation for the short-period *P*:*S* ratio is possible, however, when comparing data recorded at only one station. Also, small chemical explosions ($M_L = 3.0$) can be distinguished from most earthquakes using this method, but only at nearer ($D < 200$ km) distances. No better separation of event types was obtained by plotting E_{spPz}:E_{spSz} versus magnitude.

The scattering effects discussed here directly affect the phases presently used for regional seismic discrimination (P, S, and L_g). Consequently, this issue should be addressed in future related regional discrimination studies.

Although such scattered energy is problematic for time-domain or spectral discriminants that use short-period phases since it will possibly mask the source character, it can be useful in identifying shallow events. TERRAscope observations of local earthquake sequences clearly show that shallow earthquakes ($D < 5$ km) generate far more scattered phases and coda wave trains than do deeper events, which tend to look very "clean," i.e., contain mostly distinct, modelable phases. It may be possible to use such information as a depth discriminant for seismic monitoring purposes.

Further investigations/modifications of this discriminant may well improve it further. Applying the E_{spPz}:E_{spSz} ratio at higher frequencies ($f \geqq 4$ Hz) has been shown to improve its performance (Fig. 16). We are currently investigating the suitability of applying path corrections developed from broadband waveform modeling (Green's functions). Zhao and Helmberger (1994) have applied this technique for the purpose of developing a regional discriminant based on the deterministic modeling of seismic sources and propagation effects at broadband and short periods. Accounting for path effects also will make more direct comparisons of events possible, for example, similar magnitude events, thereby removing source scaling effects that may be inherent to these discriminants.

Once broadband Green's functions are obtained, it will be worthwhile to determine whether or not theoretical seismograms can produce similar energy ratio results. If so, these integrated wave-train energy curves can be calibrated from broadband waveform modeling. Thus, in a new geographic/tectonic region to be monitored, it will be possible to predict the behavior of earthquake and explosion energy ratios, thereby making it possible to identify potential first blasts.

Acknowledgments

This research was supported by the Air Force Office of Scientific Research under Grants F49620-93-1-0221 (Caltech) and F49620-94-C-0046 (WCFS). Contribution Number 5457, Division of Geological and Planetary Sciences, California Institute of Technology, Pasadena, California.

References

Aki, K. (1967). Scaling law of seismic spectrum, *J. Geophys. Res.* **72,** 1217–1231.

Aki, K., M. Bouchon, and P. Reasenberg (1974). Seismic source function for an underground nuclear explosion, *Bull. Seism. Soc. Am.* **64,** 131–148.

Alewine, R. W. (1972). Theoretical and observed distance corrections for Rayleigh-wave magnitude, *Bull. Seism. Soc. Am.* **62,** 6133–6142.

Basham, P. W. (1969). Canadian magnitudes of earthquakes and nuclear explosions in south-western North America, *Geophys. J. R. Astr. Soc.* **17,** 1–13.

Baumgardt, D. R. and G. B. Young (1990). Regional seismic waveform discriminants and case-based event identification using regional arrays, *Bull. Seism. Soc. Am.* **80,** 1874–1892.

Brune, J. N. (1970). Tectonic stress and the spectra of seismic shear waves from earthquakes, *J. Geophys. Res.* **75,** 4997–5009.

Chung, D. H. and D. L. Bernreuter (1981). Regional relationships among magnitude scales, *Rev. Geophys. Space Sci.* **19,** 649–663.

Day, S. M. and K. L. McLaughlin (1991). Seismic source representation for spall, *Bull. Seism. Soc. Am.* **81,** 191–201.

Day, S. M., N. Rimer, and J. T. Cherry (1983). Surface waves from underground explosions with spall: analysis of elastic and nonlinear source models, *Bull. Seism. Soc. Am.* **73,** 247–264.

Denny, M. D. and L. R. Johnson (1991). Seismic moment estimation and the scaling of the explosion source, in *Geophysical Monograph 65: Explosion Source Phenomenology,* S. R. Taylor, H. J. Patton, and P. G. Richards (Editors), American Geophysical Union, Washington, D.C., 171–183.

Denny, M. and J. Zucca (1993). DOE non-proliferation experiment includes seismic data, *EOS* **74,** 527.

Dreger, D. S. and D. V. Helmberger (1991). Complex faulting deduced from broadband modeling of the February 28, 1990 Upland Earthquake ($M_L = 5.2$), *Bull. Seism. Soc. Am.* **81,** 1129–1144.

Evernden, J. F., W. J. Best, P. W. Pomeroy, T. V. McEvilly, J. M. Savino, and L. R. Sykes (1971). Discrimination between small-magnitude earthquakes and explosions, *J. Geophys. Res.* **76,** 8042–8055.

Fliedner, M. and S. Ruppert (1994). Southern Sierra Nevada: P-wave velocity and moho depth modeling, *EOS* **75,** 585.

Gupta, I. N, W. W. Chan, and R. A. Wagner (1992). A comparison of regional phases from underground nuclear explosions at East Kazakh and Nevada Test Sites, *Bull. Seism. Soc. Am.* **82,** 352–382.

Hanks, T. C. and M. Wyss (1972). The use of body-wave spectra in the determination of seismic source parameters, *Bull. Seism. Soc. Am.* **62,** 561–589.

Haskell, N. A. (1967). Analytic approximation for the elastic radiation from a contained underground explosion, *J. Geophys. Res.* **72,** 2583–2586.

Herrin, E. and T. Goforth (1977). Phase-matched filters: applications to the study of Rayleigh waves, *Bull. Seism. Soc. Am.* **67,** 1259–1275.

Jih, R. S. (1995). Numerical investigation of relative contribution of Rg scattering and incomplete dissipation to *Lg* excitation, in *Proc. of the 17th Annual Seismic Research Symposium,* Phillips Laboratory, Hanscomb AFB, Massachusetts.

Jih, R. S. and K. L. McLaughlin (1988). Investigation of explosion generated *SV Lg* waves in 2-D heterogeneous crustal models by finite-difference method, Teledyne Geotech, AFGL-TR-88-0025, 57 pp.

Kafka, A. L. (1990). *Rg* as a depth discriminant for earthquakes and explosions: a case study in New England, *Bull. Seism. Soc. Am.* **80,** 373–394.

Kanamori, H. M., J. Mori, E. Hauksson, T. H. Heaton, L. K. Hutton, and L. M. Jones (1993). Determination of earthquake energy release and M_L using TERRAscope, *Bull. Seism. Soc. Am.* **83,** 330–346.

Kim, W.-Y., D. W. Simpson, and P. G. Richards (1993). Discrimination of earthquakes and explosions in the Eastern United States using regional high-frequency data, *Geophys. Res. Lett.* **20,** 1507–1510.

Lambert, D. G. and S. S. Alexander (1971). Relationship of body and surface wave magnitudes for small earthquakes and explosions, Teledyne Geotech, ARPA-TR-72-1714, 24 pp.

Lieberman, C. R. and P. W. Pomeroy (1969). Relative excitation of surface waves by earthquakes and underground explosions, *J. Geophys. Res.* **74,** 1575–1590.

Lilwall, R. C. (1988). Regional m_b:M_S, *Lg*/*Pg* amplitude ratios and *Lg* spectral ratios for criteria distinguishing between earthquakes and explosions: a theoretical study, *Geophys. J.* **93,** 137–147.

Lynnes, C. S., R. Baumstark, R. K. Cessaro, and W. W. Chan (1990). *Pg*/*Lg* discrimination in the western United States, Teledyne Geotech, GL-TR-90-0167, 35 pp.

Marshall, P. D. (1970). Aspects of the spectral differences between earthquakes and underground explosions, *Geophys. J. R. Astr. Soc.* **20,** 397–416.

Marshall, P. D., A. Douglas, and J. A. Hudson (1971). Surface waves from underground nuclear explosions, *Nature* **234,** 8–9.

Mayeda, K. M. and W. R. Walter (1996). Moment, energy, stress drop, and source spectra of western United States earthquakes from regional coda envelopes, *J. Geophys. Res.* **101,** 11195–11208.

Mueller, R. A. and J. R. Murphy (1971). Seismic characteristics of underground nuclear detonations: Part I. Seismic spectrum scaling, *Bull. Seism. Soc. Am.* **61,** 1675–1692.

Müller, G. (1973). Seismic moment and long-period radiation of underground nuclear explosions, *Bull. Seism. Soc. Am.* **63,** 847–857.

Murphy, J. R. and T. J. Bennett (1982). A discrimination analysis of short-period regional seismic data recorded at Tonto Forest Observatory, *Bull. Seism. Soc. Am.* **72,** 1351–1366.

Patton, H. J. (1988). Source models of the HARZER explosion from regional observations of fundamental-mode and higher mode surface waves, *Bull. Seism. Soc. Am.* **78,** 1133–1157.

Patton, H. J. and S. R. Taylor (1984). Q structure of the Basin and Range from surface waves, *J. Geophys. Res.* **89,** 6929–6940.

Patton, H. J. and W. R. Walter (1993). Regional moment: magnitude relations for earthquakes and explosions, *Geophys. Res. Lett.* **20,** 277–280.

Peppin, W. A. and T. V. McEvilly (1974). Discrimination among small magnitude events on Nevada Test Site, *Geophys. J. R. Astr. Soc.* **37,** 227–243.

Pomeroy, P. W., W. J. Best, and T. V. McEvilly (1982). Test ban treaty verification with regional data—a review, *Bull. Seism. Soc. Am.* **72,** S89–S129.

Savino, J. L., L. R. Sykes, R. C. Lieberman, and P. Molnar (1971). Excitation of seismic surface waves with periods of 15 to 70 seconds for earthquakes and underground explosions, *J. Geophys. Res.* **76,** 8003–8020.

Smith, K. D. and J. N. Brune (1993). A sequence of very shallow earthquakes in the Rock Valley fault zone; Southern Nevada Test Site (abstract), *EOS* **74,** 417.

Stead, R. J. and D. V. Helmberger (1988). Numerical-analytical interfacing in two dimensions with applications to modeling NTS seismograms, *Pure Appl. Geophys.* **128,** 101–193.

Stevens, J. L. and S. M. Day (1985). The physical basis of m_b:M_S and variable frequency magnitude methods for earthquake/explosion discrimination, *J. Geophys. Res.* **90,** 3009–3020.

Stevens, J. L. and K. L. McLaughlin (1988). Analysis of surface waves from the Novaya Zemlya, Mururoa, and Machitka test sites, and maximum likelihood estimation of scalar moments from earthquakes and explosions, S-Cubed, SSS-TR-89-9953, 80 pp.

Stump, B. W. (1985). Constraints on explosive sources with spall from near-source waveforms, *Bull. Seism. Soc. Am.* **75,** 1312–1325.

Taylor, S. R. and G. E. Randall (1989). The effects of spall on regional seismograms, *Geophys. Res. Lett.* **16,** 211–221.

Taylor, S. R., D. D. Denny, E. S. Vergino, and R. E. Glaser (1989). Regional discrimination between NTS explosions and western U.S. earthquakes, *Bull. Seism. Soc. Am.* **79,** 1142–1176.

Thio, H. K. and H. Kanamori (1995). Moment tensor inversion for local earthquakes using surface waves recorded at TERRAscope, *Bull. Seism. Soc. Am.* **85,** 1021–1038.

Vidal, A. and L. Munguia (1991). Local magnitude and source parameters for earthquakes in the Peninsular Ranges of Baja California, Mexico, *Bull. Seism. Soc. Am.* **81,** 2254–2267.

Viecelli, J. A. (1973). Spallation and the generation of surface waves by an underground nuclear explosion, *J. Geophys. Res.* **78,** 2475–2487.

Walter, W. R., K. M. Mayeda, and H. J. Patton (1995). Phase and spectral ratio discrimination between NTS earthquakes and explosions. Part I: Empirical observations, *Bull. Seism. Soc. Am.* **85,** 1050–1067.

Woods, B. B. and C. K. Saikia (1994). Regional surface wave magnitude and moment determination methods applied to nuclear explosions at the Nevada Test Site: implications for yield estimation and seismic discrimination, in *Proc. of the 16th Annual Seismic Research Symposium,* Phillips Laboratory, Hanscomb AFB, Massachusetts.

Woods, B. B., S. Kedar, and D. V. Helmberger (1993). M_L:M_0 as a regional seismic discriminant, *Bull. Seism. Soc. Am.* **83,** 1167–1183.

Zhao, L. S. and D. G. Harkrider (1992). Wave fields from an off-center explosion in an embedded solid sphere, *Bull. Seism. Soc. Am.* **82,** 1927–1955.

Zhao, L. S. and D. V. Helmberger (1994). Source estimation from broadband regional seismograms, *Pure Appl. Geophys.* **149,** 1168–1192.

Zhu, L. and D. V. Helmberger (1996). Advancement in source estimation techniques using broadband regional seismograms, *Bull. Seism. Soc. Am.* **86,** 1634–1641.

Woodward Clyde Federal Services
Pasadena, California 91101
(B.B.W.)

Seismological Laboratory
California Institute of Technology
Pasadena, California 91125
(D.V.H.)

Manuscript received 5 November 1994.